Direct Numerical Simulations of dual fuel non-premixed autoignition

E. Demosthenous*, E. Mastorakos, R. S. Cant

Department of Engineering, University of Cambridge

Trumpington Street, Cambridge CB2 1PZ, UK

Tel: +44 1223 332641

Fax: +44 1223 339906

Email: ed398@cam.ac.uk

Presented at the Ninth Mediterranean Combustion Symposium, June 2015, Rhodes, Greece.

Accepted for publication at Combustion Science and Technology.

Direct Numerical Simulations of dual fuel non-premixed autoignition

Elena Demosthenous[1], Epaminondas Mastorakos[1], Robert Stewart Cant[1]

[1] *Hopkinson Laboratory, Engineering Department, University of Cambridge, UK*

Abstract

Autoignition of turbulent methane/air mixing layers, in which n-heptane droplets have been added, was investigated by DNS. This configuration is relevant to dual-fuel, pilot-ignited natural gas engines under direct injection conditions. Two passive scalars were introduced in order to describe the dual fuel combustion. It was shown that the pre-ignition phase is dominated by n-heptane oxidation while methane oxidation is less intense. During the pre-ignition phase the methane/air mixing layer is distorted due to turbulence creating regions around the n-heptane droplets allowing the transport of intermediate species to the methane reaction zone. According to the passive scalars introduced, it was shown that ignition occurs at mixtures rich in n-heptane vapour. Subsequently, consumption of both n-heptane and methane is rapidly increased and promoted by the high temperatures achieved. The competition of the two fuels makes autoignition retarded relative to the pure n-heptane case, but accelerated relative to the pure methane case.

Keywords: Dual fuel combustion, Autoignition, n-Heptane spray, Methane, Non-Premixed

1. Introduction

Conventional fossil fuels consisting of high molecular weight hydrocarbons are increasingly substituted by natural gas, which produces lower CO_2, NO_x, and soot emissions while maintaining high efficiencies in reciprocating engine applications (Reitz, 2013; Korakianitis et al., 2011; Amjad et al., 2011; Han et al., 2013; Srinivasan et al., 2007). However, the high octane number of natural gas (main component is methane) necessitates the introduction of an energy source in order to achieve ignition. The required energy source is often supplied by the injection of a pilot fuel with different autoignition characteristics such as diesel (Korakianitis et al., 2011; Srinivasan et al., 2007; Iida et al., 1997). The majority of previous studies investigating gas-fuelled and pilot-ignited combustion have been conducted with injection of natural gas in the intake manifold followed by direct injection of the pilot fuel (Papagiannakis and Hountalas, 2004; Iida et al., 1997; Schlatter et al., 2012). It was found that the ignition delay of the pilot spray and OH* chemiluminescence intensity

is increased in the presence of methane indicating an active role of methane in the combustion process (Papagiannakis and Hountalas, 2004; Schlatter et al., 2012; Lee et al., 2003).

Apart from port injection, which gives a fully premixed methane-air mixture at the moment of the pilot fuel injection, natural gas can also be injected directly into the cylinder in order to avoid reductions in volumetric efficiency while maintaining the diesel injection to initiate combustion (Korakianitis et al., 2011). Previous studies have focused on global quantities such as engine power output and emission levels (McTaggart-Cowan et al., 2007, 2010). Nevertheless, the details of the phenomena occurring in such dual-fuel non-premixed autoignition processes have not been studied and it is unclear whether the conclusions from studies in port injection of methane are valid in the context of direct injection.

The aim of the present study is to provide physical understanding on the behaviour of the dual fuel autoignition processes when both fuels have inhomogeneous distribution. The focus is to reveal the ignition mechanism and effect of each fuel towards the other with regards to ignition. In this context, Direct Numerical Simulations (DNS) of turbulent methane-air mixing layers that include n-heptane droplets are performed under high pressures and temperatures therefore mimicking compression-ignition conditions in dual-fuel, pilot-ignited natural gas reciprocating engines.

2. Mathematical formulation

2.1. Liquid-phase governing equations

The governing equations have been described previously in DNS of spark ignition (Neophytou et al., 2011, 2012) and autoignition of turbulent sprays (Borghesi et al., 2013) and are briefly presented here. The liquid phase consisted of dilute n-heptane droplets, treated using a Lagrangian point-source formulation. The motion of each droplet is affected by the aerodynamic drag force only. The temperature within the droplet was assumed to be uniform. The droplet evaporation rate and the amount of heat exchanged with the gaseous phase was evaluated based on the thin film assumption (subscript f) and the physical properties in the thin film were computed according to the 1/3 rule. For each droplet d, a system of equations was solved in order to determine its position $\mathbf{x}_d$, velocity $\mathbf{v}_d$, diameter a_d and temperature T_d (Abramzon and Sirignano, 1989):

$$\frac{d\mathbf{x}_d}{dt} = \mathbf{v}_d \tag{1}$$

$$\frac{d\mathbf{v}_d}{dt} = \frac{\mathbf{u}\left(\mathbf{x}_d, t\right) - \mathbf{v}_d}{\tau_d^v} \tag{2}$$

$$\frac{da_d^2}{dt} = -\frac{a_d^2}{\tau_d^p} \tag{3}$$

$$\frac{dT_d}{dt} = \frac{1}{\tau_d^T}\left[T(\mathbf{x}_d,t) - T_d - B_{T,d}\frac{L_v}{W_F c_P^F}\left(\frac{T_{\rm crit}-T_d}{T_{\rm crit}-T_{\rm ref}}\right)^{0.38}\right] \tag{4}$$

where $\mathbf{u}\,(\mathbf{x}_d,t)$, $T(\mathbf{x}_d)$ are the gaseous-phase velocity and temperature evaluated at the droplet location, $T_{\rm ref}$ is the boiling temperature at the reference pressure $P_{\rm ref}$, $T_{\rm crit}$ the critical temperature, $L_{\rm u}$ the molar latent heat of evaporation and $W_{\rm F}$ the molar weight of the fuel. The relaxation times τ_d^v, τ_d^p and τ_d^T and droplet Spalding numbers for heat and mass transfer, $B_{m,d}$ and $B_{T,d}$ are evaluated here according to Abramzon and Sirignano (Abramzon and Sirignano, 1989). The fuel considered is n-heptane ($\rho_{\rm L} = 684\,{\rm kg/m^3}$, $P_{\rm ref} = 1\,{\rm bar}$, $T_{\rm ref} = 371.58\,K$, $T_{\rm crit} = 540.15\,K$, $L_v = 31.80\,{\rm kJ/mol}$).

2.2. Gaseous-phase governing equations

The temporal and spatial evolution of the gaseous phase is described by the continuity of mass, momentum, internal energy and N_s-1 transport equations for conservation of species mass fractions, with N_s being the number of species for which transport equations are solved (Neophytou et al., 2012; Borghesi et al., 2013; Jenkins and Cant, 1999).

$$\frac{\partial \rho}{\partial t} + \frac{\partial \rho u_j}{\partial x_j} = \Gamma_m \tag{5}$$

$$\frac{\partial \rho u_i}{\partial t} + \frac{\partial \rho u_i u_j}{\partial x_j} = -\frac{\partial P}{\partial x_i} + \frac{\partial \tau_{ij}}{\partial x_j} + \Gamma_{u_i} \tag{6}$$

$$\frac{\partial \rho E}{\partial t} + \frac{\partial \rho u_j E}{\partial x_j} = -\frac{\partial P u_j}{\partial x_j} + \frac{\partial \tau_{ij} u_i}{\partial x_j} - \frac{\partial q_j}{\partial x_j} + \Gamma_E \tag{7}$$

$$\frac{\partial \rho Y_\alpha}{\partial t} + \frac{\partial \rho u_j Y_\alpha}{\partial x_j} = -\frac{\partial \rho V_{\alpha,j} Y_\alpha}{\partial x_j} + \dot{\omega}_\alpha + \Gamma_{Y_\alpha} \tag{8}$$

The viscous stress tensor (τ_{ij}) and the heat flux vector (q_j) are given by the following equations:

$$\tau_{ij} = \mu\left(\frac{\partial u_i}{\partial x_j} + \frac{\partial u_j}{\partial x_i}\right) - \frac{2}{3}\mu\delta_{ij}\frac{\partial u_m}{\partial x_m} \tag{9}$$

$$q_j = -\lambda\frac{\partial T}{\partial x_j} + \sum_{\alpha=1}^{N_s}\rho V_{\alpha,j} Y_\alpha h_\alpha \tag{10}$$

where $V_{\alpha,j}$ is the diffusion velocity of species α and is evaluated according to Fick's law, modified so as to ensure consistency between the species and continuity equations:

$$V_{\alpha,j}Y_\alpha = -D_\alpha \frac{\partial Y_\alpha}{\partial x_j} + \left(\sum_{\beta=1}^{N_s} D_\beta \frac{\partial Y_\beta}{\partial x_j} \right) Y_\alpha \tag{11}$$

Equations 5-8 were closed using the following equation of state:

$$P = \rho R T \sum_{\alpha=1}^{N_s} \frac{Y_\alpha}{W_\alpha} \tag{12}$$

Where R is the universal gas constant, W_α the molecular mass, and h_α the specific enthalpy of species α. The thermal conductivity λ is evaluated according to the following expression:

$$\frac{\lambda}{c_P} = A \left(\frac{T}{T_{\text{ref}}} \right)^r$$

where $A = 2.58 \times 10^{-5}\,\text{J}\,\text{kg}^{-1}\text{m}^{-1}\text{s}^{-1}$, $T_{\text{ref}} = 298\,\text{K}$, $r = 0.7$, and $c_P = \sum_{\alpha=1}^{N_s} c_{P,\alpha} Y_\alpha$. The molecular dynamic viscosity is calculated using the Prandtl number Pr, which was set equal to 0.7. The diffusion coefficient of species α was calculated using the Lewis number Le, assumed to be unity.

The liquid source terms in eq. 5-8 are given below (Rotexo-Softpredict-Cosilab, 2009):

$$\Gamma_m = -\frac{1}{V} \sum_d \alpha_d \frac{dm_d}{dt} \tag{13}$$

$$\Gamma_{u_i} = -\frac{1}{V} \sum_d \alpha_d \frac{dm_d v_{d,i}}{dt} \tag{14}$$

$$\Gamma_E = -\frac{1}{V} \sum_d \alpha_d \left(c_P^L m_d \frac{T(\mathbf{x}_d, t) - T_d}{\tau_d^T} + \frac{dm_d}{dt} h_F(T_d) + \frac{1}{2} \frac{dm_d v_{d,i}^2}{dt} \right) \tag{15}$$

$$\Gamma_{Y_\alpha} = \delta_{\alpha F} \Gamma_m \tag{16}$$

where m_d is the mass of droplet, $h_F(T_d)$ is the fuel vapour enthalpy at the droplet surface and V the volume of the cell at the droplet location. The Kronecker delta, $\delta_{\alpha F}$, is equal to unity for the fuel species and 0 otherwise. The function α_d distributes the liquid source terms to the gas phase up to a cut-off set equal to $2a_{d,0}$ with $a_{d,0}$ being the initial Sauter mean diameter of the spray. This function decreases exponentially with increasing distance from the center of the droplet.

2.3. Numerical procedure

The three-dimensional compressible DNS code SENGA2, previously used in a variety of turbulent combustion problems (Neophytou et al., 2012; Borghesi et al., 2013; Dunstan and Jenkins,

2009; Borghesi, 2012), was implemented for solving the governing equations. A tenth-order explicit central difference scheme (Kennedy and Carpenter, 1994) was used to evaluate the first and second order spatial derivatives. Periodic boundary conditions were applied in all spatial directions, therefore mimicking a constant volume configuration. Operator splitting between transport in physical space and chemistry was implemented, enabling the calculation of stiff chemistry. Application of operator splitting in DNS has been studied and validated previously (Najm et al., 1998; Knio et al., 1999). A fourth-order, low-storage explicit Runge-Kutta scheme (Kennedy et al., 2000) with a time step $\Delta t = 5.0 \times 10^{-9}$ s was employed for advancing the gaseous and liquid phase transport equations. The gas-phase chemical reactions were advanced in time using the implicit solver VODPK (Brown et al., 1989). The time step was chosen to be smaller than the acoustic time scale in a grid cell ($\Delta x/\sqrt{\gamma(R/W_{air})T}$), representing the smallest non-chemical time scale in the simulation.

2.4. Chemical mechanism

The Liu et al. (2004) reduced mechanism was implemented containing 22 non steady-state species and 18 global steps. The mechanism was derived from a skeletal mechanism consisting of 43 species and 185 reactions. The reduced scheme was validated in terms of the ignition delay time for homogeneous mixtures at different equivalence ratios, temperatures and pressures from the experimental data of Ciezky and Adomeit (1993). It has also been used for non-premixed autoignition problems (Borghesi et al., 2013; Neophytou et al., 2012; Wright et al., 2010; Borghesi et al., 2011) and contains methane.

2.5. Simulation parameters and problem setup

In the present simulations, the cubic domain under investigation had a length of $L = 2.4$ mm and grid resolution 23 μm resulting in 104 grid nodes in each direction. The initial ambient temperature was $T = 1300$ K and the pressure was $P = 24$ bar which is lower than what is normally encountered in real diesel engines, but it is also below the critical pressure of n-heptane enabling the implementation of a simple evaporation model. Similar pressure values were previously used in DNS of spray autoignition (Borghesi et al., 2013) and experimental investigations of dual fuel engines (Papagiannakis and Hountalas, 2004). The turbulent velocity field was initialised according to the Batchelor and Townsend (1948) energy spectrum. The integral length scale was $L_{11} = L/6$ and the initial turbulent velocity fluctuations were equal to $u'_0 = 0.7\,\mathrm{m/s}$. The turbulence was isotropic and decaying, and there was no initial mean flow. The initial values of the Kolmogorov length scales were $\eta_K = 25.2\,\mu$m, indicating that gaseous-phase turbulence was well resolved.

The n-heptane droplets were randomly distributed in a sphere with its centre located at the centre of the domain and of radius $R = 0.23L$. The initial diameter of the droplets was 25 μm, their temperature was 450 K, and their initial velocity was set equal to that of the background carrier-phase. The initial distribution of methane mass fraction (Y_{CH_4}) is given by the following function.

$$Y_{CH4} = \begin{cases} \frac{Y^0_{CH4}}{2}\left[1 + \tanh(\frac{x-x_L}{\alpha\delta})\right], & for\ x \leq 0.5L \\ \\ \frac{Y^0_{CH4}}{2}\left[1 - \tanh(\frac{x-x_R}{\alpha\delta})\right], & for\ x > 0.5L \end{cases} \tag{17}$$

Essentially the Y_{CH_4} extends in the x-direction creating two mixing layers located equally spaced from $L/2$, at x_L and x_R respectively, with $x_R - x_L = 0.3L$. In the above formulation, Y^0_{CH4} is the maximum mass fraction of methane encountered across this distribution and is equal to 1, $\alpha = N\Delta x$, where N is the number of grid points, and δ is the characteristic mixing layer thickness, equal to 0.018. The configuration is shown in Fig. 1. The amount of the spray chemical energy compared to the total chemical energy of the system was set to 5 %. It was previously shown that the pressure rise due to n-heptane combustion is significantly reduced for low fractions of the spray chemical energy (Demosthenous et al., 2015).

In the particular case of dual-fuel combustion involving two hydrocarbon fuels, two passive scalars are needed in order to describe the various compositions appearing in the mixture. The first passive scalar, ξ_1, is defined based on the nitrogen mass fraction and it is equivalent to the conventional mixture fraction; it ranges from 0 in the oxidizer stream to 1 in the fuel stream.

$$\xi_1 = \frac{Y_{N_2} - Y^{ox}_{N_2}}{Y^f_{N_2} - Y^{ox}_{N_2}} \tag{18}$$

In the above definition Y_{N_2} is the local mass fraction of N_2, $Y^{ox}_{N_2}$ is the mass fraction of N_2 in the oxidizer stream, and $Y^f_{N_2}$ is the mass fraction of N_2 in the fuel stream.

In order to distinguish the contribution of each fuel, we introduce $\xi_{2,H}$ so that for each ξ_1 there is a $\xi_{2,H}$ which ranges from 0 as if the fuel present is solely methane to 1 as if the fuel present is solely n-heptane. Namely,

$$\xi_{2,H} = \frac{h - h_2(\xi_1)}{h_1(\xi_1) - h_2(\xi_1)} \tag{19}$$

where $h_1(\xi_1)$ is the enthalpy of a n-heptane/air mixture at ξ_1, $h_2(\xi_1)$ is the enthalpy of a methane/air

mixture at ξ_1, and h is the local enthalpy given by the following definition:

$$h = \sum_{\alpha=1}^{N} Y_\alpha h_\alpha \tag{20}$$

3. Results and discussion

3.1. Homogeneous reactor calculations

Homogeneous reactor calculations are essential for providing insights on the ignition delay and favourable mixture fraction value for ignition. For the particular case of dual fuel combustion under direct injection conditions it is necessary to obtain the ignition characteristics for both fuels. Thus homogeneous reactor calculations are performed for n-heptane/air and methane/air mixtures. The temperature of the air stream was 1300 K while the temperature of the fuel was 450 K and the ambient pressure was 24 bar as in the DNS investigation. The initial composition and temperature in mixture fraction space is given by assuming inert mixing between the fuel (methane or n-heptane) and the oxidizer stream (air). In addition to these conditions, homogeneous reactor calculations were also performed for the special case when the fuel stream consists both of methane and n-heptane so that $Y_{CH_4}(\xi = 1) = 0.5$ and $Y_{C_7H_{16}}(\xi = 1) = 0.5$. This mixture is denoted as B in the following. Ignition was defined as the time when the temperature exceeds 1450 K. Setting a different value of temperature cut-off would not cause any appreciable change in the ignition delay time due to the rapid increase of temperature at ignition. The resulting trends of ignition delay time (τ_{id}) are given in Fig. 2 as a function of mixture fraction. The mixture fraction value that corresponds to the shortest ignition delay time is denoted as most reactive mixture fraction (ξ_{MR}). The values of τ_{id} and ξ_{MR} for the cases investigated are given in Table 1.

The shortest ignition delay time of methane is significantly longer than the corresponding delay time of n-heptane as presented in Table 1 and this is reflected to Fig. 2 considering a greater range of mixture fraction values. Additionally, the ξ_{MR,CH_4} is leaner compared to $\xi_{MR,C_7H_{16}}$. The $\xi_{MR,C_7H_{16}}$ is leaner than what previously observed for n-heptane autoignition (Borghesi et al., 2013) due to the higher temperatures encountered in the present simulations resulting in more active lean mixtures. As Table 1 and Fig. 2 reveal, the behaviour of mixture B is not falling exactly between what is observed when the fuel is pure n-heptane or pure methane. Instead it exhibits a behaviour closer to the n-heptane, leading to the conclusion that n-heptane is dominant for determining autoignition. Furthermore, the ignition delay time of a mixture consisting of the same amount of n-heptane as

what is initially present at the $\xi_{MR,B}$ is 0.327 ms, which is shorter than τ_{id} for B. This suggests that the methane present in the mixture participates actively during the pre-ignition period and this competition between the two fuels increases the ignition delay time of the mixture.

3.2. DNS Results

3.2.1. Pre-ignition phase

During the pre-ignition phase, droplet evaporation and mixing promoted by turbulence are the dominant processes but in this particular case, due to the high temperature of the oxidizer stream, the reaction rates are also significant. Figure 3 illustrates scatter plots of heat release rate (HRR), reaction rates of C_7H_{16}, CH_4, CH_2O and of $\xi_{2,H}$ against ξ_1 at t=0.320 ms. Higher heat release rates are observed for $\xi_1 \leq 0.15$ which is consistent with the higher C_7H_{16} and CH_2O reaction rates observed at those mixture fraction values. The n-heptane is being consumed while intermediates such as CH_2O are being produced. A more complex behaviour is observed for methane which is simultaneously produced and consumed, albeit with lower consumption rate than n-heptane. To elaborate on this behaviour, a scatter plot of the reaction rate of n-heptane against the corresponding value of methane suggests that methane is produced for high consumption rates of n-heptane while it is consumed for intermediate and low values.

The mixing processes for the problem under investigation not only involves mixing between each fuel and the oxidizer stream but also mixing between the fuels. The mixing between the two fuels described by $\xi_{2,H}$ is plotted in Fig. 3 as a function ξ_1. The rich mixtures primarily consisted of methane ($\xi_{2,H} \approx 0$) rather than n-heptane because a significant amount of n-heptane needs to be evaporated in order to create rich mixtures at the instant shown. Therefore the n-heptane richer mixtures ($\xi_{2,H} \approx 1$) barely reach $\xi_1 = 0.25$ whereas methane contributes for the whole range of ξ_1.

Contours of C_7H_{16} and CH_2O mass fractions and CH_4 reaction rate are shown in Fig. 4 taken at $z = 0.5L$ at t =0.320 ms. The heptane droplets were initially located within the methane zone, but gradually evaporation and droplet motion allows n-heptane vapour to come in contact with air at the sides of the mixing layer. The methane/air mixing layers are distorted due to turbulence creating pockets surrounding the n-heptane droplets. Evaporation is stronger for the droplets that interact with the hot oxidizer stream and once significant amount of n-heptane has evaporated, intermediate species such as CH_2O are produced. Formaldehyde is also found at the interfaces of methane and hot air and although at lower concentrations this suggests that methane is also undergoing its own (slower) autoignition. The alternate behaviour of consumption and production of methane observed

in Fig. 3 for lean mixtures is clearly captured in these contour plots showing methane production at locations where n-heptane is present, while methane consumption is promoted at the interfaces of methane and the hot oxidizer.

In order to investigate the competition of the two fuels in producing intermediate species, scatter plots of the reaction rate of CH_2O is plotted in Fig. 5 against reaction rates of C_7H_{16} and CH_4. Production of CH_2O is maximized for high consumption rates of C_7H_{16} which coincides with production rates of CH_4 as CH_4 constitutes one of the intermediate species of the C_7H_{16} oxidation. As previously captured in Fig. 3 consumption of CH_4 is also associated with production of CH_2O but at lower production rates.

The behaviour of the system during the pre-ignition phase in ξ_1-$\xi_{2,H}$ space is illustrated in Fig. 6 showing shaded contours of C_7H_{16} and CH_4 reaction rates and CH_2O mass fraction. It is evident that consumption rate of C_7H_{16} is found for high values of $\xi_{2,H}$ as compositions with high $\xi_{2,H}$ values correspond to a predominantly n-heptane/air mixture. Similarly, CH_4 is being consumed for mixtures with low value of $\xi_{2,H}$ which primarily involve methane/air mixtures. Production of CH_4 coincides with consumption of C_7H_{16}. Formaldehyde is mainly found at compositions with high values of $\xi_{2,H}$.

3.2.2. Ignition phase

Based on the definition given earlier, i.e. $T > 1450$ K, ignition occurs at t=0.435 ms at $\xi_1 =$ 0.038, $\xi_{2,H}$=0.948. Ignition is therefore favoured at regions rich in n-heptane vapour. Figure 7 shows scatter plots of temperature, HRR, and reaction rates of C_7H_{16} and CH_4 taken at t=0.445 ms. The consumption rate of methane is rapidly increasing during ignition whereas the reaction rate of C_7H_{16} has not changed significantly as it was already high during the pre-ignition phase.

Figure 8 captures an ignition site showing contours of the temperature, $Y_{C_7H_{16}}$ and reaction rates of C_7H_{16} and CH_4 at $z = 0.6L$ at t=0.445 ms. Isolines of RR.CH_4 mark the areas of the alternate behaviour of CH_4 being simultaneously produced an consumed. It is apparent that ignition occurs inside the pockets created by the mixing layer of methane/air, inside which sufficient intermediate species exist. The intense production of intermediate species was a result of the presence of adequate amount of n-heptane as previously noted (Figs. 5 and 6). The n-heptane continues to supply the surrounding hot oxidizer with intermediate species but at the vicinity of the droplets the temperature is lower due to evaporative cooling (see Fig. 8). When the intermediate species reach the methane reaction zone, the oxidation of methane is promoted. Methane production is still evident at the

vicinity of n-heptane consumption at intermediate temperatures.

3.2.3. Post-ignition phase

After ignition, the temperature is increasing and propagates to leaner and richer mixtures and radicals such as OH start to be significant. Figure 9 shows scatter plots of HRR, temperature and OH mass fraction at t=0.520 ms. It is evident that there exist regions of the flow where $\xi_1 \approx \xi_{1,ign}$ but the temperature remains low and hence there is minor chemical activity while endothermic reactions are also evident. In order to provide an overview of the behaviour observed, the volume integrated reaction rates of C_7H_{16}, CH_4, O_2, OH, and CH_2O are plotted in Fig. 10 against time. As previously depicted, during the pre-ignition phase consumption of C_7H_{16} is markedly more intense than consumption of CH_4 and intermediates are mainly produced due to the oxidation of C_7H_{16}. Nevertheless, consumption of both fuels is rapidly increased at ignition while consuming radicals and oxygen. Soon after ignition their consumption subsequently drops due to the competition of both fuels to be oxidized and the endothermic reactions occurring at lean mixtures.

4. Conclusions

Autoignition of turbulent methane-air mixing layers in the presence of n-heptane sprays was investigated by DNS, in an effort to understand the fundamental flame initiation process in pilot-ignited direct-injection methane compression ignition engines. Two passive scalars were introduced for the description of dual fuel combustion. It was found that during the pre-ignition phase, intermediate species are primarily produced by the n-heptane droplets surrounded by the hot oxidizer while consumption of methane is minor. The methane/air mixing layers are distorted due to turbulence creating pockets around the droplets that facilitate transport of intermediate species to the vicinity of the methane reaction zone. Ignition occurs at lean mixtures as predicted by homogeneous reactor calculations with the n-heptane-methane case igniting closer to the n-heptane compared to the methane case. The DNS shows that autoignition occurs in locations rich in n-heptane vapour as suggested by the mixture parameters introduced to describe dual fuel combustion. Thus the ignition kernel is located where the liquid fuel has migrated towards the hot air zone, thereby reducing the delaying effect of the methane on the heptane autoignition process and increasing the evaporation rate. Subsequently after ignition, consumption of both fuels is rapidly increased and eventually a methane-air flame is established.

References

Abramzon, B., Sirignano, W.A., 1989. Droplet vaporization model for spray combustion calculations. Int. J. Heat Mass Transfer 32, 1605–1618.

Amjad, A., Saray, R.K., Mahmoudi, S., Rahimi, A., 2011. Availability analysis of n-heptane and natural gas blends in hcci engines. Energy 36, 6900–6909.

Batchelor, G., Townsend, A., 1948. Decay of turbulence n the final period. Proc. R. Soc. Lond. Ser. A 194, 527–543.

Borghesi, G., 2012. Autoignition in turbulent two-phase flows. Ph.D. thesis. Unversity of Cambridge. United Kingdom.

Borghesi, G., Mastorakos, E., Cant, R.S., 2013. Complex chemistry chemistry dns of n-heptane sprays at high pressure and intermediate temperature conditions. Combust. Flame 160, 1254–1275.

Borghesi, G., Mastorakos, E., Devaud, C., Bilger, R., 2011. Modeling evaporation effects in conditional moment closure for spray autoignition. Combust. Theory Model. 15, 725–752.

Brown, P., Byrne, G., Hindmarsh, A., 1989. Vode: A variable coefficient ode solver. J. Sci. Stat. Comput. 10, 1038–1051.

Ciezky, H., Adomeit, G., 1993. Shock-tube investiation of self ignition of n-heptane-air mixtures under engine-relavant conditions. Combust. Flame 93, 421–433.

Demosthenous, E., Borghesi, G., Mastorakos, E., Cant, R.S., 2015. Direct numerical simulations of premixed methane flame initiation by pilot n-heptane spray autoignition. Combust. Flame, doi:10.1016/j.combustflame.2015.09.013 .

Dunstan, T., Jenkins, K., 2009. The effect of hydrogen substitution on turbulent premixed methane-air kernels usng diract numerical simulation. Int. J. Hydrogen Energy 34, 8389–8404.

Han, X., Zheng, M., Wang, J., 2013. Fuel suitability in low temperature combustion in compression ignition engines. Fuel 109, 336–349.

Iida, N., Nakamura, M., Ohashi, H., 1997. Study of diesel spray combustion in an ambient gas containing hydrocarbon using a rapid compression machine. SAE Paper 970899.

Jenkins, K.W., Cant, R.S., 1999. Dns of turbulent flame kernels, in: Proc. 2nd AFOSR Conf. DNS LES, Kluwer Academic Publishers.

Kennedy, C., Carpenter, M., 1994. Several new numerical methods for compressible shear-layer simulations. Appl. Numer. Math. 14, 397–433.

Kennedy, C., Carpenter, M., Lewis, R., 2000. Low-storage, explicit runge-kutta schemes for compressible navier-stokes equations. Appl. Numer. Math. 35, 177–219.

Knio, O.M., Najm, H.N., Wyckoffy, P.S., 1999. A semi-implicit numerical scheme for reacting flow ii: Stiff, operator-split formulation. J. Comput. Phys. 154, 428–467.

Korakianitis, T., Namasivayam, A., Crookes, R., 2011. Natural-gas fuelled spark-ignition (si) and compression-ignition (ci) engine performance and emissions. Prog. Energy. Combust. Sci. 37, 89–112.

Lee, C.S., Lee, K.H., Kim, D.S., 2003. Experimental and numerical study on the combustion characteristics of partially premixed charge compression ignition engine with dual fuel. Fuel 82, 553–560.

Liu, S., Hewson, J.C., Chen, J.H., Pitsch, H., 2004. Effect of strain rate on high-pressure nonpremixed n-heptane autoignition in counterflow. Combust. Flame 137, 320–339.

McTaggart-Cowan, G.P., Jones, H.L., Rogak, S.N., Bushe, W.K., Hill, P.G., Munshi, S.R., 2007. The effects of high-pressure injection on a compressionignition, direct injection of natural gas engine. J. Eng. Gas Turbines Power 129, 579–588.

McTaggart-Cowan, G.P., Rogak, S.N., Munshi, S., Hill, P., Bushe, W.K., 2010. The influence of fuel composition on a heavy-duty, natural-gas direct-injection engine. Fuel 89, 752–759.

Najm, H.N., Wyckoff, P.S., Knio, O.M., 1998. A semi-implicit numerical scheme for reacting flow i: Stiff chemistry. J. Comput. Phys. 143, 381–402.

Neophytou, A., Mastorakos, E., Cant, R.S., 2011. Complex chemistry simulations of spark ignition in turbulent sprays. Proc. Combust. Inst. 33, 2135–2142.

Neophytou, A., Mastorakos, E., Cant, R.S., 2012. The internal structure of igniting turbulent sprays as revealed by complex chemistry DNS. Combust. Flame 159, 641–664.

Papagiannakis, R., Hountalas, D., 2004. Combustion and exhaust emission characteristics of a dual fuel compression ignition engine operated with a pilot diesel fuel and natural gas. Energy Conv. Manag. 45, 2971–2987.

Reitz, R., 2013. Directions in internal combustion engine research. Combust. Flame 160, 1–8.

Rotexo-Softpredict-Cosilab, 2009. GmbH and Co. KG Bad Zwischenahn (Germany), Cosilab Collection, Version 3.0. www.SoftPredict.com.

Schlatter, S., Schneider, B., Wright, Y.M., Boulouchos, K., 2012. Experimental study of ignition and combustion characteristics of a diesel pilot spray in a lean premixed methan/air charge using a rapid compression expansion machine. SAE Paper 010825.

Srinivasan, K.K., Krishnan, S.R., Qi, Y., Midkiff, K.C., Yang, H., 2007. Analysis of diesel pilot-ignited natural gas low-temperature combustion with hot exhaust gas recirculation. Combust. Sci. Technol. 179, 1737–1776.

Wright, Y.M., Margari, O., Boulouchos, K., De-Paola, G., Mastorakos, E., 2010. Experiments and simulations of n-heptane spray auto-ignition in a closed combustion chamber at diesel engine conditions. Flow Turbul. Combust. 84, 49–78.

Table 1: Homogeneous reactor calculations

Fuel	τ_{id} [ms]	ξ_{MR}
C_7H_{16}	0.225	0.037
CH_4	2.079	0.015
B=0.5C_7H_{16}+0.5CH_4	0.463	0.033

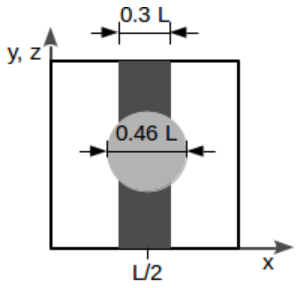

Figure 1: Schematic of the configuration in the DNS investigation. Dark grey shows the methane layer which is homogeneous in the y- and z-directions. The n-heptane droplets were initially located in a sphere (light grey).

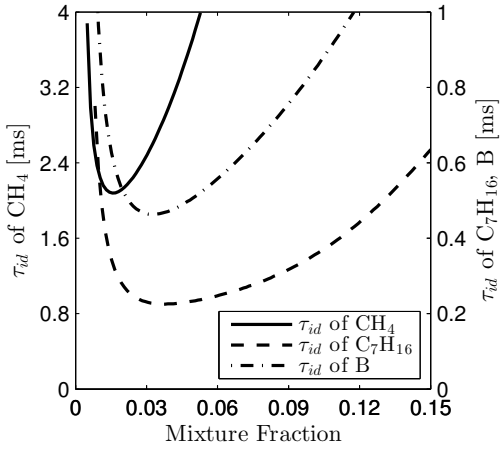

Figure 2: Ignition delay time of homogeneous n-heptane/oxidizer, methane/oxidizer and n-heptane-methane/oxidizer (B=$0.5C_7H_{16}$+$0.5CH_4$) mixtures. The temperature of the oxidizer ($\xi = 0$) is 1300 K and of the fuel ($\xi = 1$) is 450 K and $P = 24$ bar.

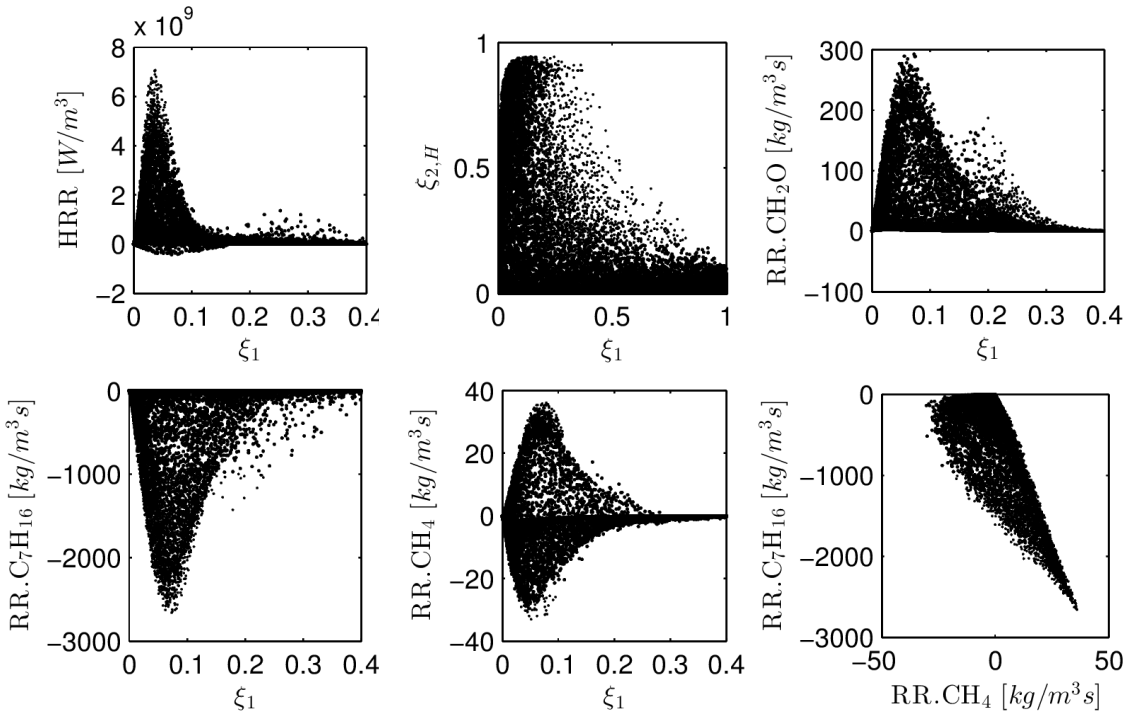

Figure 3: Scatter plots of heat release rate (HRR), $\xi_{2,H}$, reaction rates of CH_2O, C_7H_{16}, and CH_4 against ξ_1, and reaction rates of C_7H_{16} against CH_4 at t=0.320 ms.

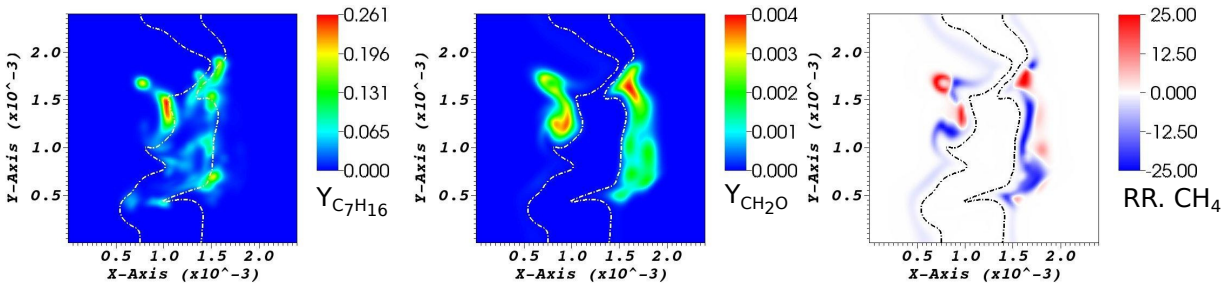

Figure 4: Contour plots of C_7H_{16} and CH_2O mass fractions and reaction rate of CH_4. The iso-line of ξ_1=0.5 is also shown (dotted line). The contours are taken at $z = 0.5L$ at $t = 0.320$ ms.

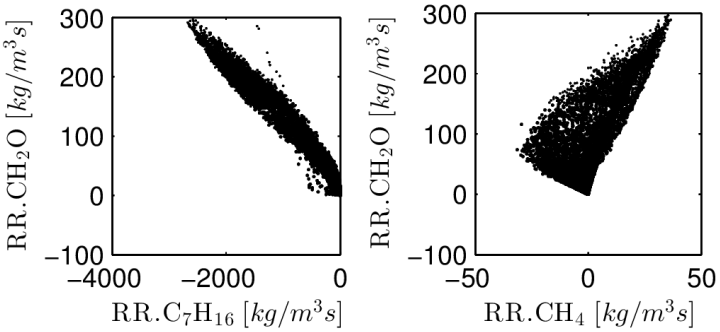

Figure 5: Scatter plots of reaction rate of CH_2O against reaction rate of C_7H_{16} and CH_4 at t=0.320 ms.

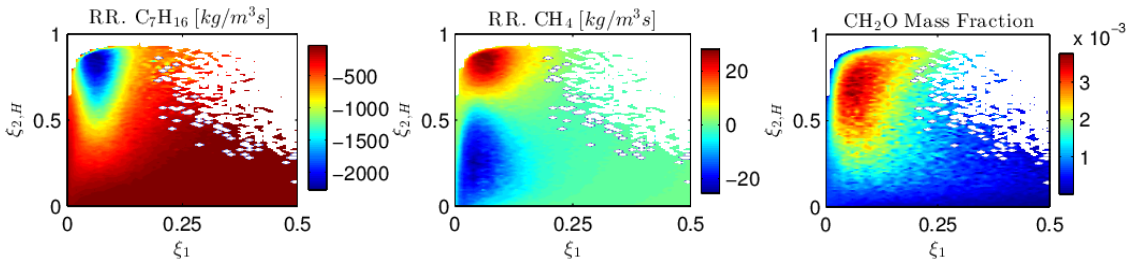

Figure 6: Contours of C_7H_{16} and CH_4 reaction rates and CH_2O mass fraction in ξ_1 - $\xi_{2,H}$ space at t=0.320 ms.

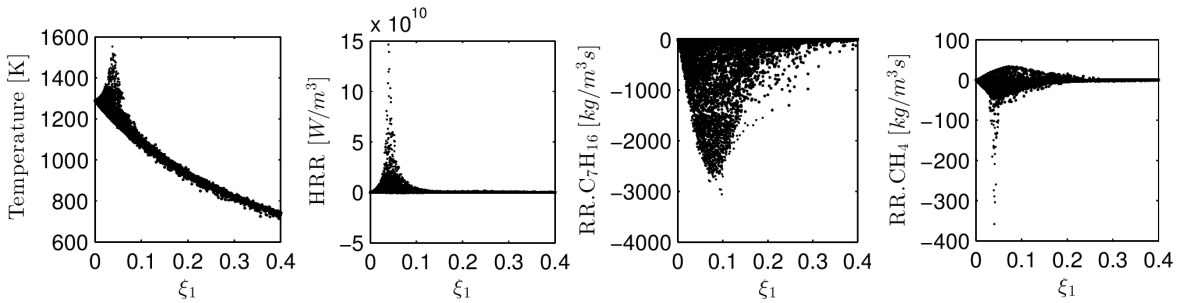

Figure 7: Scatter plots of temperature, heat release rate (HRR) and reaction rates of n-heptane and methane against ξ_1 at $t = 0.445$ ms.

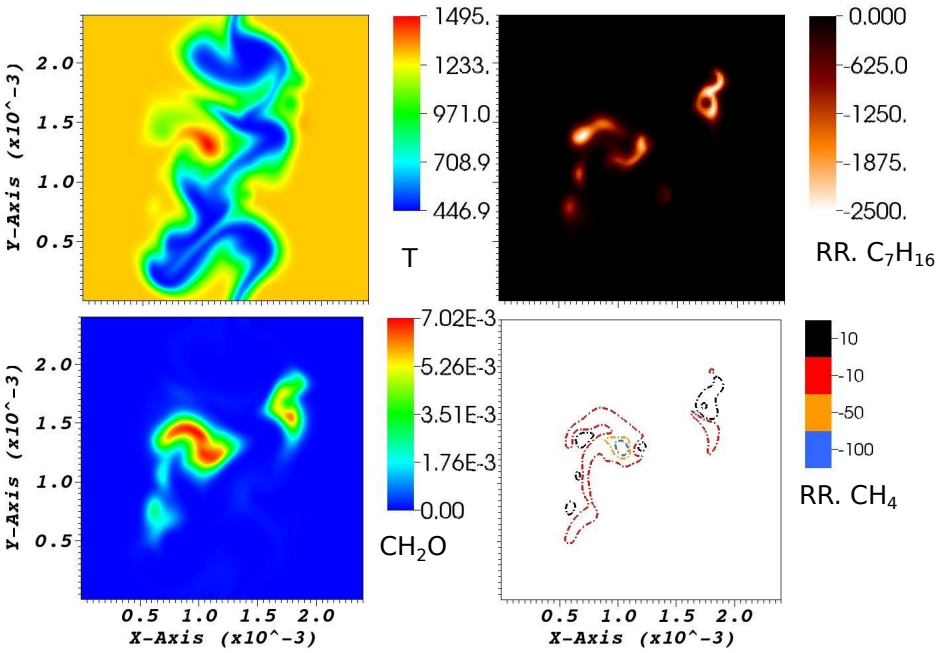

Figure 8: Contour plots of temperature, reaction rates of n-heptane and methane and mass fraction of CH_2O taken at z=0.6L at t =0.445 ms.

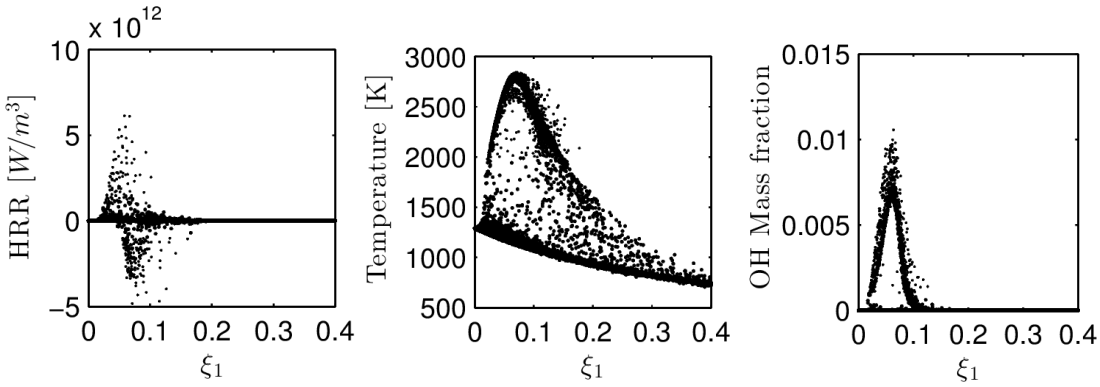

Figure 9: Scatter plots of heat release rate (HRR), temperature and OH mass fraction at $t = 0.520$ ms.

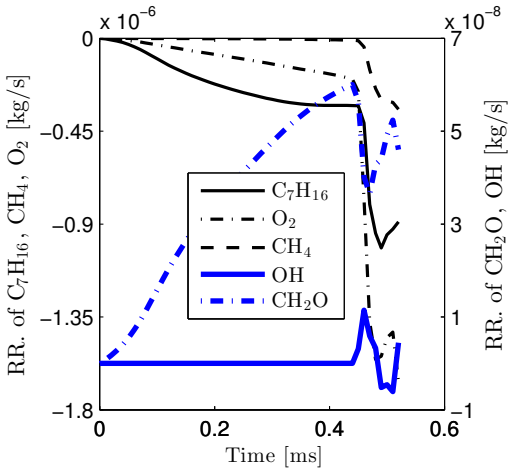

Figure 10: Temporal evolution of the volume integrated reaction rates of C_7H_{16}, CH_4, O_2, OH, and CH_2O.

List of Figures